P6.15   RADAR ANALYSIS OF THE AIRFLOW OVER GEOGRAPHIC FEATURES THAT MAY AFFECT MESOCYCLONE INTENSITY AND TORNADOGENESIS

Timothy A. Coleman* and Kevin R. Knupp
The University of Alabama, Huntsville, Alabama

1. INTRODUCTION

It may be shown that horizontal gradients in roughness length and associated friction, with some component normal to the low level wind, produce quasistationary areas of horizontal shear, and associated vertical vorticity and circulation. In a nearly neutral boundary layer, this vorticity may be detected at significant heights above ground level. The intensity of mesocyclones passing across these gradients in friction may be altered, in some cases leading to tornadogenesis, and in other cases weakening the mesocyclone significantly.

In addition, the channeling or tunneling of flow in river valleys, gorges, and other such topographic features may also locally change the wind direction and speed, affecting the storm-relative helicity and/or producing quasistationary regions of vertical vorticity. Bosart et al. (2004) and LaPenta et al. (2005) have examined the effects of wind channeling in tornado cases in the northeastern United States.

In this paper, Doppler radar data will be used to examine quasistationary regions of positive or negative vertical vorticity or storm-relative helicity associated with horizontal gradients in friction and others associated with flow channeling. Where available, dual-Doppler synthesis will be used.   However, dual-Doppler coverage is not widespread at the present time, and a simple method has been developed for examining quasi-stationary perturbations to the background flow, and associated vertical vorticity, using a single Doppler radar. This method differs from other, more complex single Doppler radar wind field retrievals (e.g., Bluestein and Hazen 1989; Rinehart 1979; Sun et al. 1991; Liou et al. 1991; Qiu and Xu 1992). It may be shown using the horizontal momentum equation, in the case of along-wind gradients in friction, the wind speed adjusts to the change in friction much more rapidly than the wind direction does, due to the small magnitude of the Coriolis force relative to the drag force. Therefore, VAD wind profiles are used to determine the wind direction at each range and height over the lowest elevation scan of a radar, and wind speeds and vectors are calculated assuming this wind direction estimate. These wind fields are then averaged over multiple volume scans to remove noise and the effect of individual convective elements, producing a map of the average wind at low levels, usually over a 2-3 hour period. Areas of background vorticity may then be located, and the effect upon storms interacting with these areas can be

Corresponding Author Address: Timothy A. Coleman, Atmospheric Science Department, The University of Alabama in Huntsville, 320 Sparkman Drive, Huntsville, AL 35805; Email: coleman@nsstc.uah.edu.

examined. For wind tunneling effects, a similar method is used, except available surface wind data and DEM elevation data are used to estimate the wind direction in channeling areas, and regions of background vorticity are located.   Several case studies will also be presented.

2. THEORY

a. Horizontal gradients in roughness length

The roughness length, z_0, is a parameter used to describe the roughness of the land surface and how this roughness affects the frictional drag on the wind and the associated vertical wind profile in the planetary boundary layer (PBL).   In general, larger values of roughness length correspond to lower near-surface winds and larger wind shear, especially in the surface layer (e.g., Garratt 1992; Tennekes 1973; Blackadar and Tennekes 1968).   Large horizontal gradients in roughness length most commonly occur along
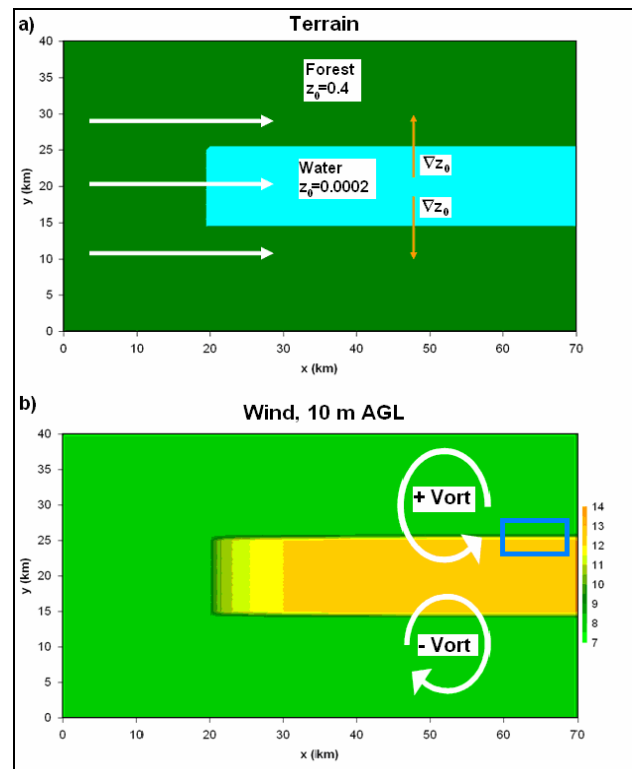

Figure 1. Schematic in the (x, y) plane of 10 m AGL flow from a forest to a body of water with forest on both sides of the water. a) Roughness lengths (z_0, m), wind vectors (white arrows), and the gradient of z_0 (orange arrows). b) 10 m AGL wind speed (m s^{-1}) and regions of vertical vorticity.

boundaries between water and land. However, smaller gradients in z_0 may also occur near other discontinuities in land cover type, including forests, cropland, and urban areas (e.g., Garratt 1993; Grimmond and Oke 1999).

When the low level wind blows with a component normal to a horizontal gradient in z_0, horizontal shear, and therefore vertical vorticity, may be produced. The vorticity is positive (negative) when the roughness length gradient is directed toward the left (right) of the wind vector (see Figure 1). This production of vorticity is explained mathematically through the often-ignored friction term in the vorticity equation (e.g., Bluestein 1992):

$$\frac{D\zeta}{Dt} = \hat{k} \cdot \nabla \times \vec{F}_{friction} \ . \ (1)$$

Applying Equation 1 to Figure 1, the friction force is directed toward the left, since the wind is toward the right. Along the top edge of the area of water, the gradient of z_0 is directed northward, implying that the magnitude of the friction force increases with y also. This means that $\nabla \times F$, or the curl of the friction force, points upward (in the positive z-direction), in the same direction as the unit vector k. Therefore, the dot product in Equation 1 is positive, and the vertical vorticity tendency is positive. Along the bottom edge of the water, ∇z_0 is southward, and $\nabla \times F$ points in the negative z-direction. There, the dot product is negative, implying a negative vorticity tendency.

It should also be noted that, when the wind also has component parallel to the horizontal gradient in z_0, the low-level wind speed and vertical shear of air moving from one z_0 to another does not adjust to the new z_0 instantly. This adjustment occurs over some distance (e.g., Bergstrom 1986), and this is also shown in Figure 1.

The horizontal scale over which the wind increases as a function of y determines the *vorticity*. In the idealized case shown in Figure 1, since roughness length is a piecewise function of x and y, the wind speed is discontinuous at the upper and lower boundaries of the water. Therefore, in theory, the vorticity would have an infinitely large magnitude there. In the real atmosphere, however, mixing in a neutral boundary layer with winds greater than 5 m s^{-1} would produce some horizontal momentum flux away from the water, causing a continuous transition of the wind speed from the water into the forest, and a finite vorticity magnitude. Also, the wind rarely blows exactly perpendicular to the gradient in roughness length over any significant distance, also allowing a continuous wind speed field and finite vorticity. Even in an idealized situation like the case shown in Figure 1, where the wind speed is discontinuous producing infinite vorticity, the total *circulation* produced is independent of the horizontal scale of the wind change. To calculate the circulation C around the blue rectangle in Figure 1b,

$$C = \oint_{BR} \vec{V} \cdot d\vec{l} = u_{bottom}\delta x + v_{right}\delta y -$$

$$u_{top}\delta x - v_{left}\delta y \ . \ (2)$$

Since $v = 0$, and δx is constant for any given rectangle, only the difference between u_{bottom} and u_{top} determines the circulation, with C being independent of δy.
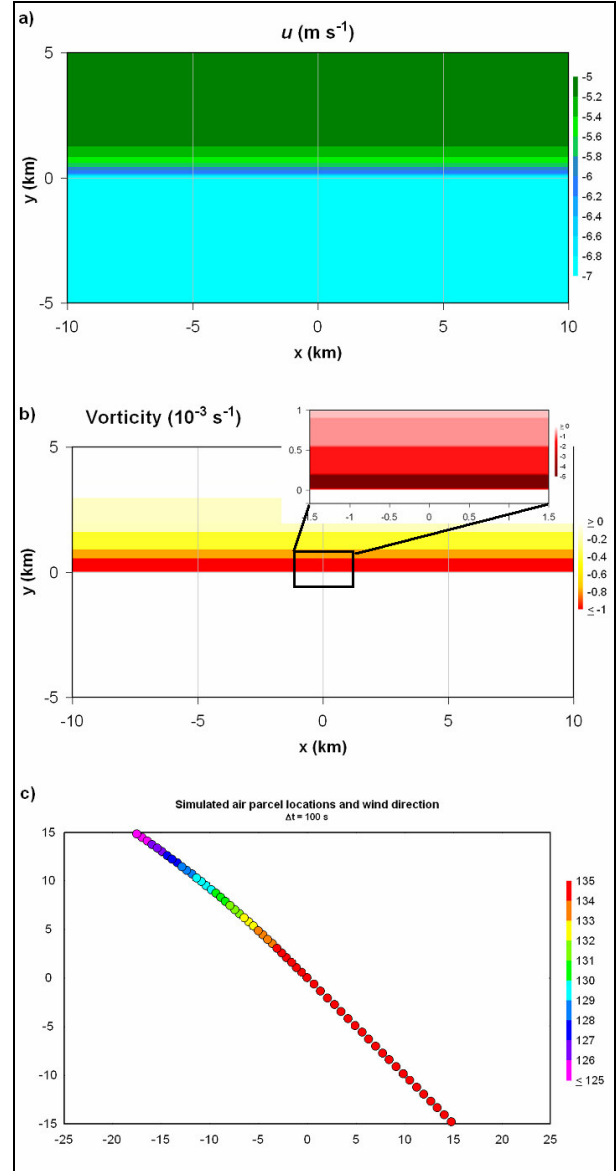

Figure 2. a) u-component of wind (m s^{-1}), b) vorticity (10^{-3} s^{-1}) and c) parcel location and wind direction ($y = 0$ at coastline) for simulation described above. In part b, note inset has different scale than main plot.

A numerical simulation was performed to quantify the circulation and vorticity produced at an abrupt change in roughness length. Suppose a southeasterly wind (from 135 degrees) at 10 m s^{-1} (u_0 = -7.07 m s^{-1}, v_0 = 7.07 m s^{-1}) at 10 m AGL blows from over a smooth water surface (z_0 = 0.0002 m), past an east-west oriented coastline and onto a forest (z_0 = 0.4 m). The x- and y- components of the Coriolis force over the water may be readily calculated, and assuming the wind is in geostrophic balance over the water, the pressure gradient force may be determined also. Geostrophic balance begins to break down over the forest. The rate of decrease of the wind speed is calculated at each time step by adapting empirically determined coefficients from Bergstrom (1986). The wind speed at 10 m AGL decreases quickly immediately after crossing the coastline, dropping to about 7.5 m s^{-1} after 1.25 km of exposure over the land. The wind then decreases more slowly to 6 m s^{-1} after 15 km of exposure over land. The slower wind speeds (caused by friction) also produce smaller Coriolis accelerations, and the wind begins to turn slightly left, in the direction of the lower pressure. Eventually, the wind will regain a three-force balance including the PGF, Coriolis, and frictional forces.

Figure 2 shows u, vorticity ζ, and the actual track of an individual parcel (along with its wind direction) for the simulation described above, in (x, y) coordinates. (The changes in wind speed, u and v are functions of y only, so $\partial v/\partial x = 0$ and $\zeta = - \partial u/\partial y$.) Consistent with the discussion above, most of the change in wind speed due to friction occurs within 2 km of the coastline. Even though the change in u over the first 5 km over the forest is only about 2.2 m s^{-1}, the rapid nature of the decrease produces a narrow band of fairly significant negative vorticity near the coastline. The magnitude of the vorticity is larger than 10^{-3} s^{-1} within about 0.5 km of the coastline, and as large as 5 x 10^{-3} s^{-1}, similar to the magnitude of the vorticity in a weak mesocyclone (e.g., Dowell et al. 1997). The circulation around a box, 10 km on each side, centered along the coastline, is -2.2 x 10^4 m^2 s^{-1}.

b. Wind channeling

It has been shown in numerous studies that near-surface winds tend to be "channeled," or flow roughly parallel to the axis of a relatively deep valley, such as the Tennessee, Hudson, Rhine, and St. Lawrence Valleys (e.g., Martner and Marwitz 1982; Whiteman and Doran 1993; Carrera et al. 2009). However, as pointed out by Whiteman and Doran (1993), in statically unstable conditions, shallower valleys have less effect due to downward transport of momentum. In Figure 3, the theoretical cross-correlation between above-valley (geostrophic) and in-valley flow is shown for forced wind channeling in the Tennessee River Valley, that runs NE to SW, and compared to observations in that area. Theoretically, the winds always blow parallel to the axis of the valley. If there is any component of the geostrophic wind from the NE direction, the valley wind blows NE. The situation is similar for a SW component. The actual observations confirm the theory, showing that the observed wind observations in the valley during
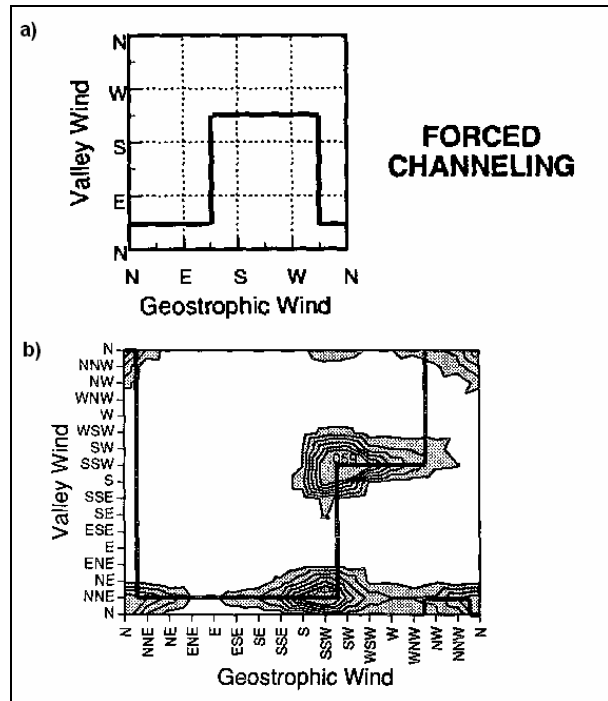

Figure 3. a) Theoretical and b) observed joint probability distributions of geostrophic and valley wind directions at Sequoyah, TN (from Whiteman and Doran 1993).

the given study period were primarily NNE or SSW, roughly along the valley axis at that location.

Wind channeling also often results in increased wind speeds in a valley or between two mountains (e.g., Martner and Marwitz 1982; Jian and Wu 2008). In severe storm environments with strong winds and vertical mixing, it is possible that the directional change in wind due to channeling and the increased wind speeds in a valley, may extend upward at least somewhat above the top of the valley. In either case, ambient vertical vorticity may be produced in a similar way to that shown in Fig. 1, with positive vertical vorticity to the left of the valley (looking downwind), and negative vertical vorticity to the right of the valley. In addition, the increased wind speeds in valleys or between mountains may locally enhance storm inflow, or produce ambient vertical vorticity downstream and to the left from the gap between the mountains (see Figure 4).

3. RADAR ANALYSIS

a. Methodology

Dual-Doppler analysis is the most effective way to use Doppler radar data to calculate horizontal gradients in wind speed and associated vorticity at discontinuities in surface roughness length or in cases of wind channeling. This method is utilized in some of the case studies in this paper. However, since this paper attempts to examine preliminary cases outside of dual-Doppler networks, a fairly simple method was used to determine the actual wind speed and direction at the
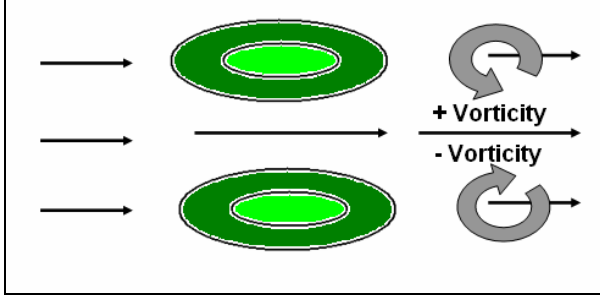
Figure 4. Idealized illustration of flow channeling between two mountains (green shading represents higher topography), a resulting jet, and corresponding downstream vorticity.

lowest available elevation angle, over all or part of the domain of a single Doppler radar, when dual-Doppler analysis was not available. This method uses the assumption that the wind direction is only a function of height AGL, and not of range nor azimuth, *over the part of the radar domain being examined*. It is also assumed, since the elevation angle of the radar is less than 1 degree, that the vertical component of motion is negligible. This method is only applicable in areas outside of wind channeling. Other methods must be used in those cases; however, estimates of the effects of wind channeling in the preliminary cases herein are provided, in at least one case using this technique.

The wind direction β is determined as a function of height using velocity azimuth display (VAD) analysis (Browning and Wexler 1968). If significant mesoscale features in the wind field, in a quadrant of the radar data away from the area being examined, contaminate the full VAD analysis, a pseudo-VAD analysis is performed using data only at the elevation angle and near the azimuth of the study area. At each data point in the radar scan, given the radial velocity V_r, wind direction β, and azimuth θ at each point, the magnitude of the wind speed is determined using the following:

$$\left| \vec{V} \right| = \frac{V_r}{\cos(\beta - \theta)} \ . \quad (3)$$

This method produces all or part of a conical slice of wind speed and direction (see Figure 3). The components of the wind u and v are then calculated at each point, using the relationships

$$u = -\left| \vec{V} \right| \sin \beta \quad (4)$$

$$v = -\left| \vec{V} \right| \cos \beta \quad (5).$$

We are examining *non-transient* variations in the flow field due to horizontal gradients in roughness length. So, the wind speed and direction over the study area, using the method described above (using radial velocity and VAD analysis for each radar scan), is calculated for several radar scans over a period of one to two hours. The wind vector at each point in the study area is then averaged over all the radar scans,

minimizing the effect of transient features in the Doppler velocity field (mesocyclones, turbulence, etc.). Once average wind vectors over a 1-2 hour period are determined, *average vorticity and circulation due to non-transient features such as topography and friction may be calculated*.

b. Error analysis

A large part of this paper involves wind vector and vorticity calculations near horizontal discontinuities in roughness length, often as air parcels move from land to water or vice versa. Therefore, one must consider the changes in wind direction associated with the changing force balance (as shown in Figure 2c). If the change in wind direction is fairly large over a short distance, especially in an area where the angle between the wind direction and the radar beam is closer to normal than parallel (causing small values of cos (β - θ) and large values of |V|/V$_r$), the single-radar method described herein produces errors. We must quantify these errors so the accuracy of this method may be verified in any given case.

The vorticity is given in natural coordinates by (adapted from Holton 2004):

$$\zeta = -\frac{\partial V}{\partial n} + V\frac{\partial \beta}{\partial s} \quad (6)$$

where *V* is the wind speed, *n* is the direction perpendicular and to the left of the wind, and $\partial\beta/\partial s$ is the change in wind direction per unit distance traveled along a streamline. The two terms on the right-hand side of Equation 6 represent the shear and curvature vorticity, respectively. Scale analysis using the numerical simulation in section 2 indicates that $\partial V/\partial n$ scales to $O(10^{-3}$ s$^{-1})$. $V \partial\beta/\partial s$ is $O(10^{-7}$ s$^{-1})$, mainly because the study area where most of the shear and vorticity were produced was very near the coastline, and changes in wind direction β over that distance were extremely small. Therefore, the curvature term may be ignored for these analyses. ∂n, in addition to V_r and θ (components of |V| in Equation 3) are measured quantities, but one must assume a wind direction β based on VAD throughout the analysis, so the effects of errors in β are the only ones that must be analyzed.

Since θ is known, the error in β - θ equals the error in β. To find the error in |V| in Equation 3, we take the derivative of Equation 3 with respect to β:

$$\frac{d\left| \vec{V} \right|}{d\beta} = \frac{V_r \tan(\beta - \theta)}{\cos(\beta - \theta)} \quad (7)$$

Now, substituting for V_r from Equation 3:

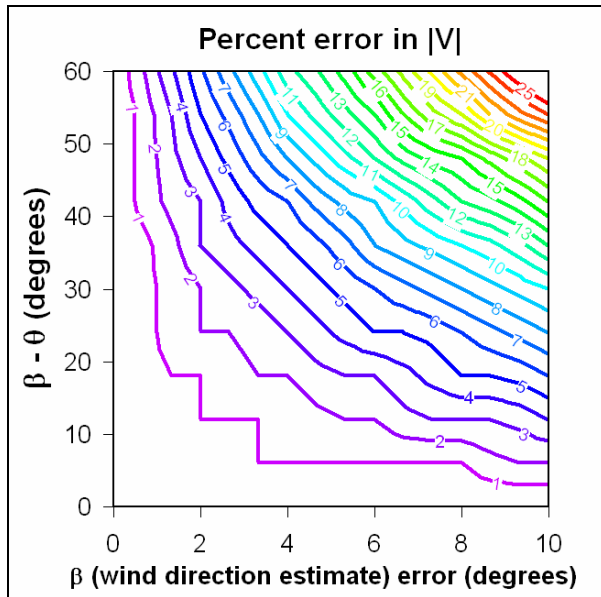$$\frac{d \ln\left| \vec{V} \right|}{d\beta} = \tan(\beta - \theta) . \quad (8)$$

Figure 5. Relative error (%) in the calculation of $|V|$, given varying values of error in β (wind direction estimate) and $\beta - \theta$ (magnitude of angle between radar beam and wind direction).

Therefore, the *relative* error in the wind speed $|V|$ per unit error in wind direction estimate is equal to the tangent of $\beta - \theta$, or proportional to the magnitude of the angle made between the radar beam and the wind direction. A plot of percent error in estimated wind speed as a function of ($\beta - \theta$) and error in estimated wind direction is shown in Figure 5. Note, for example, that for a reasonably small radar angle of view ($\beta - \theta <$ 45 degrees), errors in wind speed will be smaller than 20%, as long as the estimate of wind direction Is within 10 degrees of the actual wind direction.

Also, since vorticity here is defined as the *change in V* normal to the wind direction $\partial V/\partial n$, and since the wind direction, averaged over a 1-2 hour period, generally varies little on the meso-γ scale, any errors in the magnitude of V should be fairly consistent with respect to n, making the errors in vorticity calculations even smaller. Considering the case simulated in section 2a, most of the vorticity occurs within 1 km of the coastline. Within that region, the wind direction β only changes 0.17 degrees due to friction. For a radar located directly north from a point on the coastline, *this would only introduce a 0.3% error in the calculation of vorticity.*

4. CASE STUDIES

a. Wheeler Lake, Alabama

On 20 June 2008, an experiment was carried out to examine the thermally-forced lake breeze along Wheeler Lake in northwest Alabama. The lake is a wide (> 3 km in some locations) NW-SE nearly linearly-oriented lake along the Tennessee River, and NW flow was prevalent. The topography around the lake is negligible, with terrain height changes of less than 20 m MSL per 10 km normal to the river. The UAH Mobile Alabama X-Band (MAX) Radar was placed in a position to allow excellent dual-Doppler analysis around the lake.

Figure 6 shows the average perturbation wind vectors (at 250 m AGL) from 1900 through 2000 UTC on 10 June 2008. The thermally-direct circulation away from the cooler lake is apparent. However, there is also a significant wind perturbation in the direction of the mean wind over the water, indicating winds accelerating due to the lower friction. Vorticity is plotted in Figure 6, and consistent with Figure 1, there is positive vorticity, on the order of 10^{-3} s^{-1} along the northeast side of the lake to the left looking downwind), and negative vorticity on the southwest side of the lake.
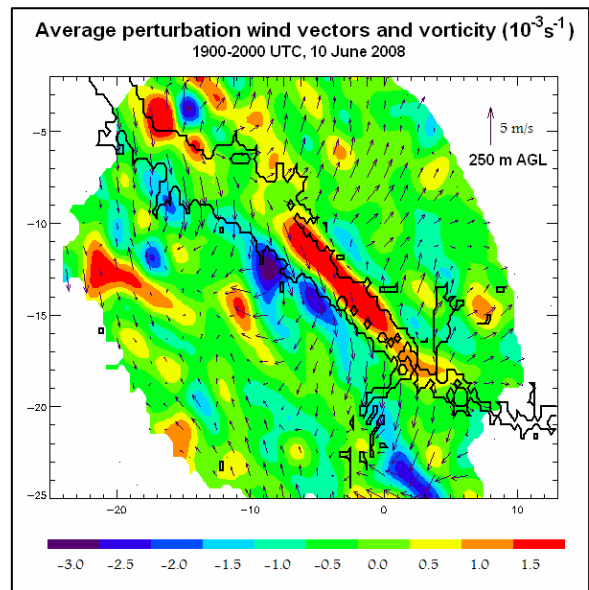

Figure 6. Dual-doppler perturbation wind vectors and vorticity (10^{-3} s^{-1}) over Wheeler Lake, 1900-2000 UTC 10 June 2008

b. Hurricane Katrina – Mississippi Coast

At 0700 UTC on 29 August 2005, the center of Hurricane Katrina was still approximately 250 km SW of the Mississippi Coast. This produced strong but fairly uniformly ENE flow along the coast. Given the horizontal gradient in roughness length, from the water to the land (south to north), wind speeds over the open water were higher than those over the land. Using the radar technique described in section 3 and data from the Slidell, LA (KLIX) WSR-88D radar, average wind speeds and directions during the 0500 through 0800 UTC timeframe along the MS coast were estimated (Figure 7). Average wind speeds decreased from 43-45 m s^{-1} about 25 km offshore to near 35 m s^{-1} just inland, with a fairly significant shear zone about 15 km offshore. An average vorticity plot based on these winds shows the zone of negative vertical vorticity just offshore, consistent with the roughness length gradient being to the right of the wind direction.
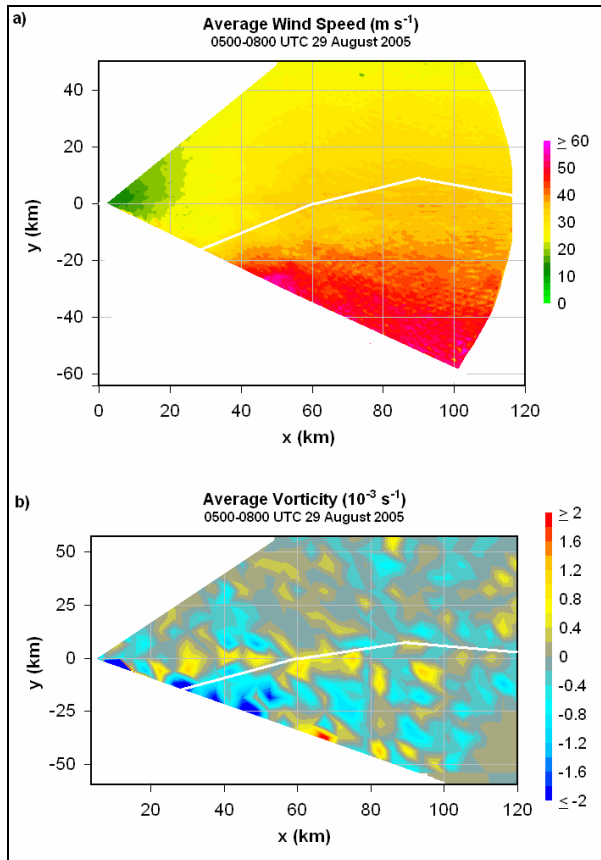
Figure 7. Radar-derived a) average wind speed (m s^{-1}) and b) vertical vorticity (10^{-3} s^{-1}) from KLIX radar, 05-08 UTC 29 August 2005. White line denotes coastline.

Between 0430 and 0600 UTC on 29 August 2005, two intense mesocyclones approached the Mississippi Gulf Coast. The radial velocity display from KLIX (Figure 8) shows the intensity of the mesocyclones at 0510 UTC, when both were still offshore. Both mesocyclones attained large amplitude peak vorticities of 2×10^{-2} s^{-1}. However, as these storms approached and crossed the coastline, encountering the area of ambient negative vorticity, the vorticity of the mesocyclones decreased significantly, and no tornadoes were reported.

c. Hurricane Katrina – Alabama Gulf Coast

Also, after the center of Hurricane Katrina was nearly 100 km inland at 1800 UTC on 29 August 2005 (located about 140 km NW of Mobile, Alabama), strong southerly flow was occurring over Mobile Bay. The technique described in section 3 was applied to the velocity data from the Mobile, AL (KMOB) WSR-88D radar from 1759 through 1859 UTC. As shown in Figure 8, winds around 40 m s^{-1} over the waters of the Gulf of Mexico and Mobile Bay decreased quickly to 35 m s^{-1} over Mobile and Baldwin Counties of Alabama, located on the west and east sides of the bay, respectively. This produced a zone of ambient positive vorticity on the western shore of Mobile Bay, and negative vorticity on
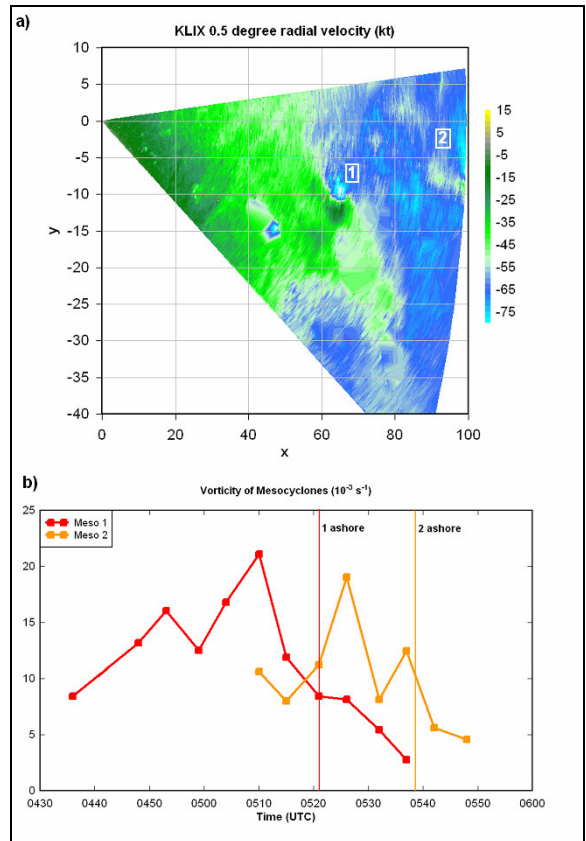

Figure 8. a) Radial velocities (kt) from KLIX at 0510 UTC 29 August 2005, showing mesocyclones 1 and 2; b) Time series of mesocyclone vorticity (10^{-3} s^{-1}) of meso 1 (red) and meso 2 (orange). Meso 1 crossed the coast at 0521 UTC, and meso 2 at 0538, as shown.

the eastern shore, again consistent with Equation 1 (see Figure 9).

d. Panama City Beach tornado, 15 September 2004

As Hurricane Ivan approached the Alabama Gulf Coast during the afternoon hours of 15 September 2004, numerous supercell thunderstorms approached the coast of the Florida panhandle. Similar to the case along the Mississippi Coast ahead of Katrina, an overall ESE flow ahead of the storm produced ambient negative vertical vorticity along the NW Florida coastline. However, at Panama City Beach, a tornado touched down within 2 km of the coastline, causing $5 million in damage and one fatality (*Storm Data*). It is possible that the Panama City Beach tornado was initiated or enhanced by positive ambient vorticity associated with a dense coastline of high-rise condominiums to the south of a lagoon and a large bay. Level 2 NEXRAD radar data were not available, but given the geometry of the beachfront condominiums relative to the bay, it seems possible that friction slowed the winds there, producing an area of positive vorticity at the southern end of the bay. This positive vorticity may have enhanced the mesocyclone in the approaching mesocyclone and caused tornadogenesis (see Figure 10).
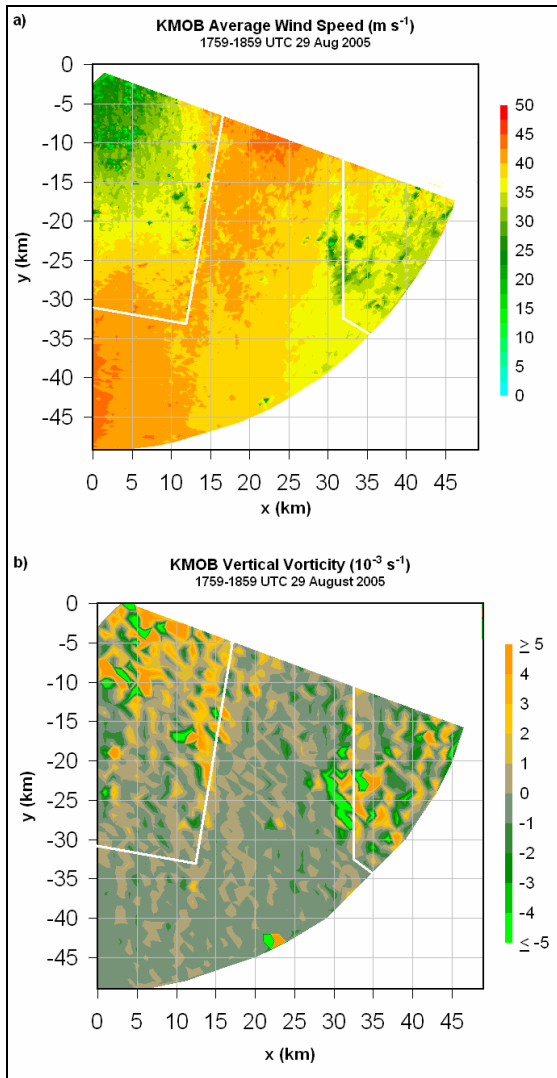
Figure 9. Radar-derived a) average wind speed (m s^{-1}) and b) vertical vorticity (10^{-3} s^{-1}) from KMOB radar, 18-19 UTC 29 August 2005. White lines denote coastline.

Figure 10. Geometry of Panama City tornado. Red squares indicate area of high-rise condos. Purple line is tornado path. White vectors are background wind.

e. Guntersville, AL tornado, 6 Feb 2008

A long-track supercell thunderstorm crossed Guntersville Lake of the Tennessee River around 1045 UTC on 6 February 2008, during the second wave of the Super Tuesday tornado outbreak. As shown in Figure 11, Guntersville Lake is oriented SW to NE, and is very large. Its width varies from 3 to 5 km over much of its greater than 50 km in length. Given the SSW low-level flow on 6 Feb 2008, the horizontal gradients in friction along the lake should set up positive vorticity on the north side of the lake, and negative vorticity on the south side.

Also, In contrast to the lack of topography in NW Alabama, the Tennessee River Valley becomes deeper in NE Alabama and east Tennessee. Even at the lower end of the Tennessee Valley in NE Alabama near Guntersville Lake, topography changes of 150 m over horizontal distances of only 4 km occur (see Figure 11b). This deep valley may be responsible for some forced channeling of the wind in the valley, increasing wind speeds and causing additional ambient vertical vorticity of the same sign as that produced by friction.

As shown by a single-radar analysis based on the Hytop, AL WSR-88D (KHTX) of the average winds between 0800 and 0930 UTC (Figure 12), a fairly significant jet is present *near the lake*, with average wind speeds about 5 m s^{-1} higher over the lake than over the surrounding land. This produces an area of positive vorticity on the north side of the lake and negative vorticity on the south side of the lake. These results could be biased somewhat if wind channeling is also occurring, changing the wind direction from the assumed VAD used in the analysis. However, channeling would still produce a vorticity pattern similar to the one shown.
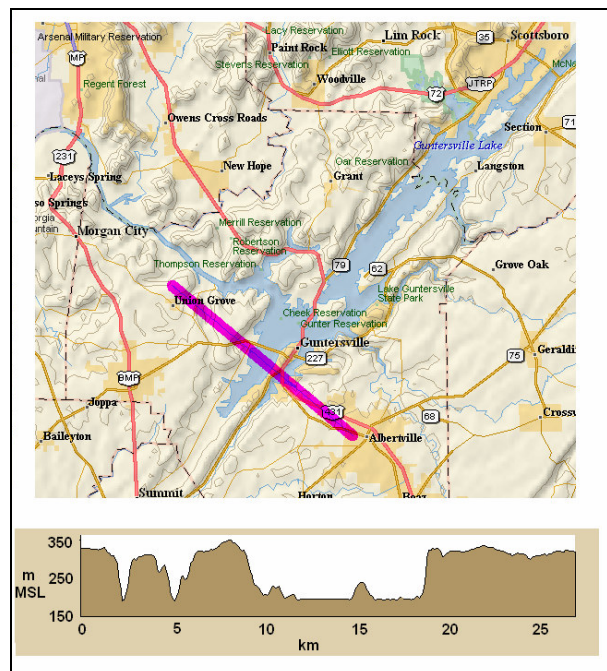

Figure 11. a) Map of Guntersville Lake; b) Cross-section of topography along line segment normal to lake
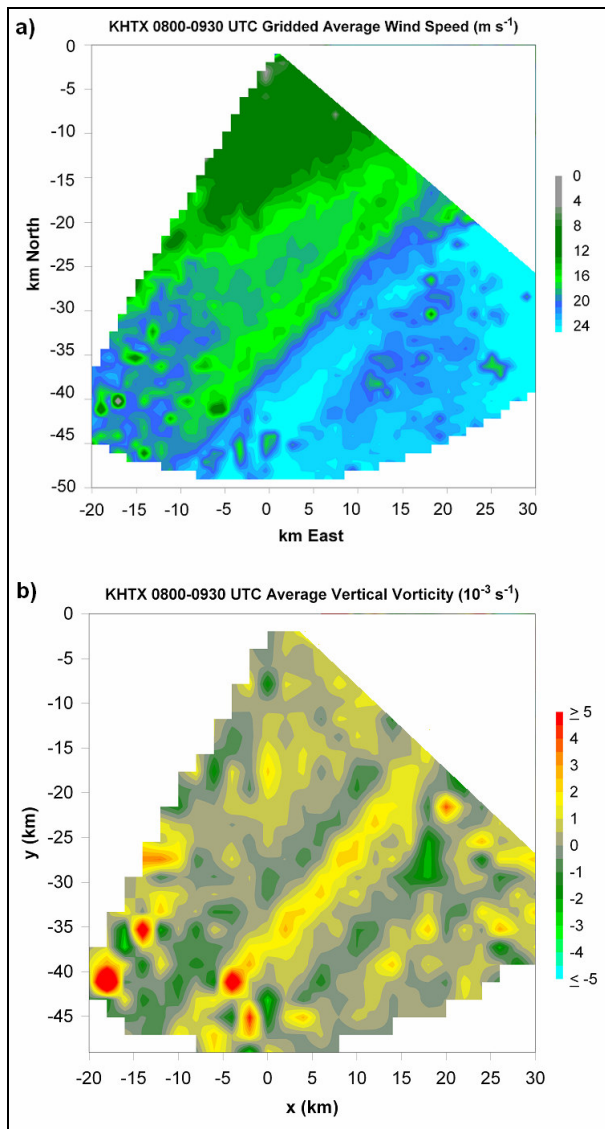
Figure 12. a) Average wind speed (m s^{-1}) from 0800 through 0930 UTC 6 Feb 2008 based on KHTX analysis; b) average vorticity (10^{-3} s^{-1})

The long-lived supercell mentioned above produced a small tornado near Cullman, AL (SW tornado along track in Figure 13) around 1000 UTC, then traveled approximately 65 km before producing another tornado on the northwest side of Lake Guntersville at 1045 UTC. This tornado quickly dissipated as it crossed the lake. It is possible that this tornado was associated with enhancement of mesocyclone vorticity by the positive background vorticity on the NW side of the river, and then the mesocyclone weakened in the area of negative background vorticity on the SE side of the river.

f. Lacey's Spring, AL tornado, 2 Apr 2009

On 2 April 2009, a thunderstorm that was part of a QLCS contained a mesocyclone and attained supercell characteristics. The storm produced a tornado near
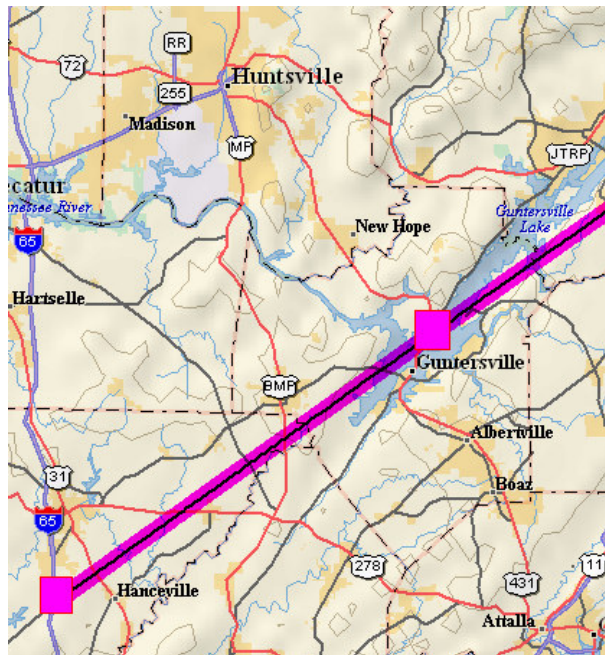

Figure 13. Track of supercell across part of NE Alabama on 6 Feb 2008. Squares indicate locations of tornadogenesis.

Lacey's Spring, AL, around the time it interacted with an apparently terrain-channeled southerly inflow jet, produced by flow between two mountain peaks less than 5 km south to the track of the mesocyclone (see Figure 14). The valley is quite steep, with the terrain dropping about 200 m MSL and rising back up again over a horizontal distance of less than 5 km.

As shown by the ARMOR Doppler radar imagery in Figure 15, a clear increase in inbound velocities, indicating enhanced southerly inflow, is present just SE of the storm at 2213 UTC. This enhanced inbound velocity increased the storm-relative helicity in the
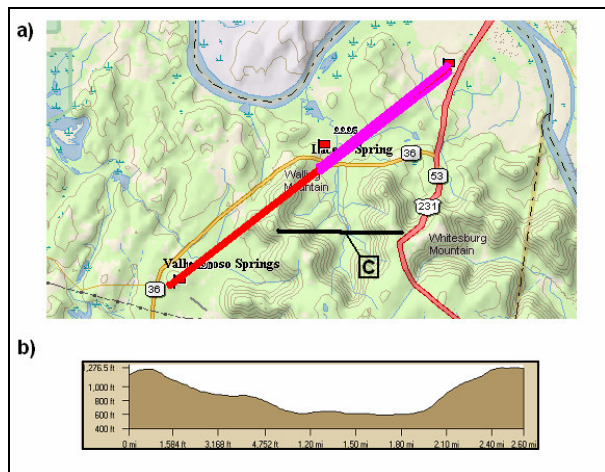

Figure 14. a) Track of supercell (red) and tornado (purple) on 2 Apr 2009. b) Cross-section of topography along cross-section C, as labeled in a).
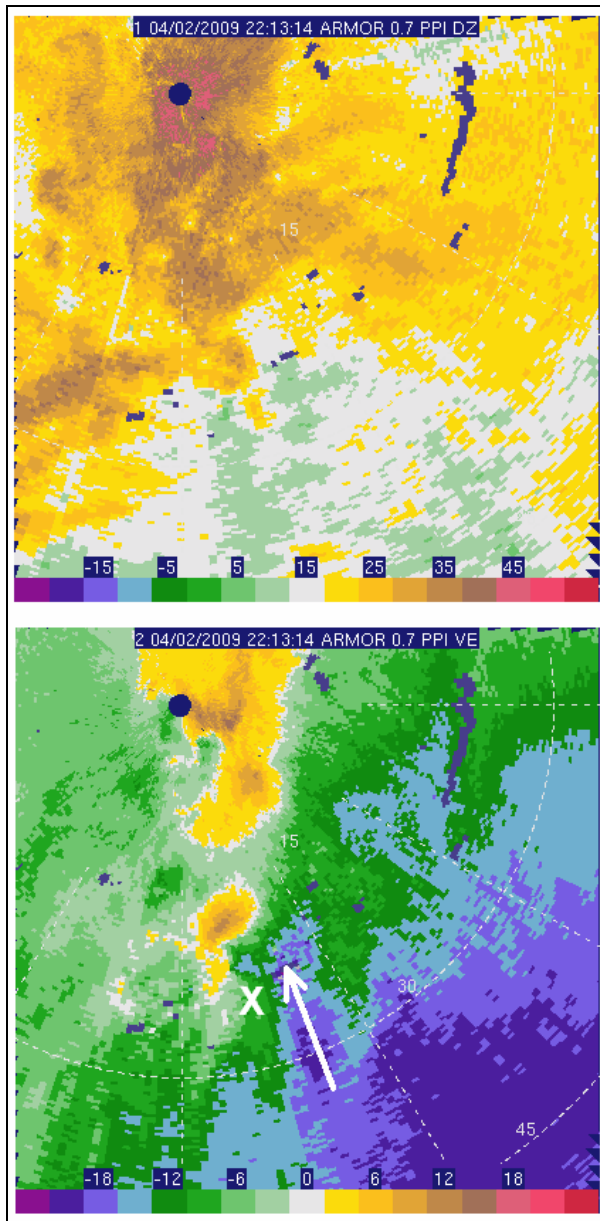
Figure 15. Reflectivity (top, dBZ) and radial velocity (bottom, m s^{-1}) from ARMOR radar at 2213 UTC. Arrow denotes enhanced inflow due to channeling between mountains, and the "X" denotes the area of possible ambient vertical vorticity due to the enhanced inflow.

storm's environment due to increased inflow speed, and may have also produced positive ambient vertical vorticity to the west of the enhanced inflow. Tornadogenesis occurred 13 minutes later at 2226 UTC.

5. CONCLUSIONS

In this paper, it was shown theoretically and through a simple numerical model, that when the low-level wind has a component normal to a horizontal gradient in the roughness length, ambient vertical vorticity and circulation are produced. The produced vorticity is positive when the gradient in roughness length z_0 points to the left of the wind vector, and is negative when ∇z_0 points to the right of the wind vector. It was also shown that, in some cases, wind channeling by flow through valleys or between mountains may not only locally enhance storm-relative helicity by increasing low-level wind speeds, but may also produce ambient vertical vorticity.

The intensity of mesocyclones passing across the vertical vorticity or enhanced storm-relative helicity produced by these topographic mechanisms may be altered. In some cases when the ambient vertical vorticity is positive and the mesocyclone intensifies, tornadogenesis may occur. In other cases, when ambient vorticity is negative, mesocyclones may weaken upon interaction with it.

Dual-Doppler analysis is preferred, but is often not available, especially when examining preliminary cases such as we are doing in this paper. A fairly simple method was developed for determining the average background wind speed and direction over certain parts of the radar domain, using several volume scans of data from one Doppler radar. This allowed calculations of ambient vertical vorticity associated with horizontal gradients in roughness length.

Several preliminary case studies demonstrate that horizontal gradients in friction may produce local regions of ambient vertical vorticity. Dual Doppler analysis of winds and vorticity along Wheeler Lake in Alabama matched up almost perfectly with the idealized simulation of wind blowing along a body of water, with positive vorticity to the left of the wind vector and negative vorticity to the right. Single-Doppler analysis showed that in the southerly flow over Mobile Bay, Alabama, well to the ESE of the center of then-inland Hurricane Katrina, winds were much higher on average over the bay than over the land, setting up background positive vorticity on the western shore of Mobile Bay, and negative vorticity on the eastern shore.

Locally-changed ambient flow and vertical vorticity appears to have affected the intensity of mesocyclones in some cases shown in this paper. ENE flow along a generally east-west coastline in Mississippi, well before the landfall of Hurricane Katrina, produced negative vorticity just offshore, and approaching mesocyclones weakened significantly upon interaction with this area of negative vorticity. Just the opposite effect may have occurred before the landfall of Hurricane Ivan, when ESE flow along the Florida Panhandle interacted with a large horizontal gradient in friction between large buildings to the south and a bay and a lagoon to the north. This could have produced background positive vorticity, and a tornado formed within 2 km of the shoreline.

It was also shown that wind channeling, in valleys and between mountains, may increase wind speeds and change the wind direction. The increased wind speed may enhance storm-relative helicity, while the speed and direction changes may produce areas of ambient vertical vorticity. On 6 Feb 2008, a long-track supercell storm, that had not produced a tornado over a fairly long

distance, produced a tornado on the northwest side of Lake Guntersville, Alabama. Single-Doppler analysis showed a significant low-level "jet" over the lake, with positive vorticity to the NW and negative vorticity to the SE. The horizontal gradient in friction between the water and the land probably played a role, but the the river valley there is also rather steep, so wind channeling may have also played a role. A rotating storm that was part of a QLCS moved just north of a fairly deep north-to-south running valley between two mountains in NE Alabama on 2 Apr 2009. Radial velocity measurements from a radar northwest of the area showed enhanced inbound velocities near the valley, likely representing channeled flow. This channeled southerly flow would have increased the storm-relative helicity, and may have produced vertical vorticity on the NW side of the valley. The rotating storm passed through the channeled flow, and produced a tornado 13 minutes later.

In order to better determine the effects of horizontal gradients in roughness length and wind channeling, field studies using Dual Doppler analysis and or synthetic dual-Doppler analysis using a mobile radar are required. This is especially true for the unstable boundary layer conditions often found around thunderstorms; however, many tornadoes in the southeastern U.S. occur during the cold season, when flow channeling may also be more prevalent. However, the theory presented in this paper is sound, and preliminary case studies are consistent with the theory. Given the potential importance of topographic features in enhancing or weakening mesocyclones, this subject requires further research. It could aide NWS forecasters in issuing tornado warnings, especially since topographic features are static, allowing "zones" of enhanced or suppressed vorticity to be analyzed before storms move into a region.

REFERENCES

Bergstrom, H., 1986: A simplified boundary layer wind model for practical application. *J. Climate. And Appl. Meteor.*, **25**, 813-824.

Blackadar, A. K., and H. Tennekes, 1968: Asymptotic similarity in neutral barotropic planetary boundary layers. *J. Atmos.. Sci.*, **25**, 1015-1020.

Bluestein, H. B., and D. S. Hazen, 1989: Doppler-radar analysis of a tropical cyclone over land: Hurricane Alicia (1983) in Oklahoma. *Mon. Wea. Rev.*, **117**, 2594-2611.

Bluestein, H. B., 1992: *Synoptic-Dynamic Meteorology in Midlatitudes*, Vol. I. Oxford, 431 pp.

Bosart, L. F., K. LaPenta, A. Seimon, and M. Dickinson, 2004: Terrain-influenced tornadogenesis in the northeastern United States: An examination of the 29 May 1995 Great Barrington, Massachusetts tornado. *Preprints, 22nd Conference on Severe Local Storms, Hyannis, MA*, 14.5, American Meteorological Society.

Browning, K.A., and R. Wexler, 1968: The Determination of Kinematic Properties of a Wind Field Using Doppler Radar. *J. Appl. Meteor.*, **7**, 105–113.

Carrera, M.L., J. R. Gyakum, and C. A. Lin, 2009: Observational study of wind channeling within the St. Lawrence River Valley. *J. Appl. Meteor. and Climatology*, in press.

Dowell, D. C., H. B. Bluestein, and D. P. Jorgensen, 1997: Airborne Doppler radar analysis of supercells during COPS-91. *Mon. Wea. Rev.,* **125,** 365–383.

Garratt, J., 1993: Sensitivity of Climate Simulations to Land-Surface and Atmospheric Boundary-Layer Treatments-A Review. *J. Climate*, **6**, 419–448.

Garratt, J. R., 1992, *The atmospheric boundary layer*. Cambridge: Cambridge University Press, 316 pp.

Grimmond, C.S.B., and T.R. Oke, 1999: Aerodynamic Properties of Urban Areas Derived from Analysis of Surface Form. *J. Appl. Meteor.*, **38**, 1262–1292.

Holton, J. R., 2004: *An Introduction to Dynamic Meteorology*. 4th ed. Academic Press, 535 pp.

Jian, G.J., and C.C. Wu, 2008: A Numerical Study of the Track Deflection of Supertyphoon Haitang (2005) Prior to Its Landfall in Taiwan. *Mon. Wea. Rev.*, **136**, 598–615.

LaPenta, K.D., L.F. Bosart, T.J. Galarneau, and M.J. Dickinson, 2005: A Multiscale Examination of the 31 May 1998 Mechanicville, New York, Tornado. *Wea. Forecasting*, **20**, 494–516.

Liou, Y. C., T. Gai-Chen, and D. K. Lilly, 1991: Retrieval of wind temperature and pressure from single Doppler radar and a numerical model. *25th International Conf. on Radar Meteorology*, Paris, Amer. Meteor. Soc., 151-154.

Martner, B.E., and J.D. Marwitz, 1982: Wind Characteristics in Southern Wyoming. *J. Appl. Meteor.*, **21**, 1815–1827.

Qiu, C.J., and Q. Xu, 1992: A Simple Adjoint Method of Wind Analysis for Single-Doppler Data. *J. Atmos. Oceanic Tech.*, **9**, 588–598.

Rinehart, R. E., 1979: Internal storm motions from a single non-Doppler weather radar. NCAR/TN-146+STR, 262 pp.

Storm Data, National Weather Service.

Sun, J., D.W. Flicker, and D.K. Lilly, 1991: Recovery of Three-Dimensional Wind and Temperature Fields from Simulated Single-Doppler Radar Data. *J. Atmos. Sci.*, **48**, 876–890.

Tennekes, H., 1973: Similarity laws and scale relations in planetary boundary layers. Chapter 5 in Workshop in Micrometeorology, D. A. Haugen, ed., pp. 177-216. Boston: American Meteorological Society.

Whiteman, C.D., and J.C. Doran, 1993: The Relationship between Overlying Synoptic-Scale Flows and Winds within a Valley. *J. Appl. Meteor.*, **32**, 1669–1682.